Applied Physics A (2021) 127:600
https://doi.org/10.1007/s00339-021-04759-4

Applied Physics A
Materials Science & Processing

Structural, magnetic, and in vitro inhibitory characteristics of Ce-substituted $MnFe_2O_4$ nanoparticles

Fatemeh Sorayyah Mohafez[1] · Abdol Mahmood Davarpanah[1] · Abbas Rahdar[2] · Hamid Beyzaei[3] · Orhan Zeybek[4] · S. D. Barrett[5]

Received: 12 February 2021 / Accepted: 13 July 2021

Abstract
$MnCe_xFe_{2-x}O_4$ ($x = 0.0, 0.6, 1.4$) nanoparticles were successfully synthesized via sol–gel method. Their structural and magnetic properties were studied using X-ray diffraction, scanning electron microscopy, energy-dispersive X-ray spectroscopy, and vibrating sample magnetometry techniques. The average crystallite size calculated using Scherrer equation was in the range of 26.90–60.44 nm. Scanning electron microscopy showed that the size of nanoparticles is less than 50 nm. Energy-dispersive X-ray results showed that the composition of the elements was relevant as expected from the synthesis. Vibrating sample magnetometry indicated that the samples have soft ferromagnetic properties. The highest saturation magnetization was related to the $MnFe_2O_4$ sample after annealing at 700 °C. The in vitro inhibitory activities of $MnFe_2O_4$ and $MnCe_{1.4}Fe_{0.6}O_4$ nanoparticles were assessed against pathogenic fungi *Aspergillus fumigatus*, *Candida albicans*, and *Fusariumoxysporum*. Acceptable antifungal effects were observed in the presence of $MnCe_{1.4}Fe_{0.6}O_4$ nanoparticles with minimum inhibition concentration and minimum fungicide concentration susceptibility determinations. As a result, these nanoparticles can be considered as potential antifungal agents.

Keywords Magnetic nanoparticles · SEM · XRD · Antifungal potential · MIC · MFC

1 Introduction

The history of ferrite materials dates back to several centuries ago when rocks with the ability to absorb iron were discovered [1]. The study of magnetic nano-ferrites using chemical methods in the presence of environmentally friendly surfactants in a simple way is an important step toward the application of this group of nanoparticles in various practical fields such as drug delivery, water treatment, etc. Naturally occurring ferrites, such as magnetite, are soft magnets. The magnetic and electrical properties of ferrite-based materials make them suitable for a wide range of applications, such as high-frequency devices, microwave components, and biomedical applications [2–4]. Manganese ferrite ($MnFe_2O_4$) belongs to a group of soft magnetic materials with high magnetic permeability, low magnetic loss, high magnetic saturation, and relatively high temperature. Recently, $MnFe_2O_4$ nanostructures have been used in many applications such as microwave devices, computer memory chips, converter antennas, catalysts, sensors, and electronic devices. The shape, size, and morphology of nanostructured spinel materials play a vital role in determining the structural, morphological, optical, electrical, and magnetic properties. Due to their amazing properties in comparison with their bulk counterparts, manganese ferrite nanostructures with different morphologies such as nanoparticles, nanorods, and nanofibers have been synthesized via different methods including thermal decomposition, solvent hydrolysis, sol–gel, coprecipitation, and microwave methods [5].

✉ Abdol Mahmood Davarpanah
a.m.davarpanah@phys.usb.ac.ir

1 Department of Physics, Faculty of Science, University of Sistan and Baluchestan, Zahedan, Iran

2 Department of Physics, Faculty of Science, University of Zabol, Zabol, Iran

3 Department of Chemistry, Faculty of Science, University of Zabol, Zabol, Iran

4 Department of Physics, Faculty of Science and Arts, Balikesir University, 18 km, Cagis Campus, Balikesir 10145, Turkey

5 Department of Physics, University of Liverpool, Liverpool L69 7ZE, UK

Published online: 17 July 2021

Rare earth metals are used as promoter for active sites formation. Rare earth cations (trivalent cations such as Ce^{3+}) affect the materials electronic distribution, favoring the adsorption of oxygen species [6–8]. So far, there is very little research on the application of these metals as dopants for the improvement of catalytic properties of ferrite materials. Therefore, in this research, cerium is considered as doping element. Cerium oxide or ceria with the unique ability to change oxidation state between + 3 and + 4 has various applications in UV absorbers, catalytic converters for car exhaust systems, solar cells, optics, and oxygen sensors [9]

The aim of this research is to prepare nanosized $MnFe_2O_4$ and Ce-doped manganese ferrite nanoparticles via sol–gel method and to study their structural and magnetic properties. The in vitro inhibitory activities of $MnFe_2O_4$ and Ce-substituted nanoparticles were also studies.

2 Experimental

2.1 Materials

Manganese nitrate [$Mn(NO_3)_2 4H_2O$] (99%, Merck), iron nitrate [$Fe(NO_3)_3.9H_2O$] (99%, Merck), cerium nitrate[$Ce(NO_3)_3.6H_2O$] (99%, Merck), and citric acid ($C_6H_8O_7.H_2O$) were used as-received without further purification.

2.2 Preparation of nano-ferrites

The first step for the synthesis of $MnCe_xFe_{2-x}O_4$ ($x = 0.0$, 0.6, 1.4) nanoparticles via sol–gel method is the preparation of an aqueous solution containing different metal nitrates by dissolving $Mn(NO_3)_2.4H_2O$, $Fe(NO_3)_3.9H_2O$, and $Ce(NO_3)_3.6H_2O$ in distilled water containing citric acid under magnetic stirring at 80 °C. At the same time, ammonia was added dropwise to the solution until the pH of the solution reached 7.0. After 3 h, a concentrated solution was formed which was poured into a crucible and heated on an electric heater until a black deposit was obtained. The powder was converted to a puffy gray powder after annealing at 700 °C for 3 h.

2.3 In vitro antifungal susceptibility test

Antifungal drugs, i.e., terbinafine hydrochloride and fluconazole, as well as RPMI 1640 (Roswell Park Memorial Institute 1640) medium buffered to pH 7.0 with morpholine propane sulfonic acid (MOPS) were purchased from Sigma-Aldrich. Pathogenic yeast, i.e., *Candida albicans* (PTCC 5027), and molds, i.e., *Fusariumoxysporum* (PTCC 5115) and *Aspergillus fumigatus* (PTCC 5009), were provided from Persian Type Culture Collection (PTCC), Karaj, Iran. Yeast and mold suspensions were prepared with concentrations of $0.5–2.5 \times 10^3$ and $0.4–5 \times 10^4$ CFU mL^{-1}, respectively. Broth microdilution and streak plate susceptibility tests were performed according to Clinical and Laboratory Standards Institute (CLSI) guidelines M27-A2, M38-A2 and M26-A [1] and the average of three independent experiments were reported.

In MIC test, 20 µL of each NP (concentrations of 10,240, 5120, 2560, 1280, 640, 320, 160, 80 µg ml^{-1}) in distilled water were added to wells 1–8 in a row of a 96-well microplate. 80 µL of RPMI 1640 and 100 µL of the prepared fungal suspensions were added to all the wells. Microplates were incubated under shaking at 100 rpm at 35 °C for 48 h. The MIC value was considered as the lowest concentration of nanoparticles (NPs) at which no visible turbidity was observed.

In MFC test, all non-turbid wells in the previous step were cultured in RPMI 1640 agar media plates. Dishes were incubated for 24 h at 35 °C at 45–55% relative humidity. The MFC was identified as the lowest concentration of NPs at which no microorganism was survived.

3 Characterization of ferrite nanoparticles

X-ray diffraction (XRD) patterns of ferrite nanoparticles were obtained by an X-ray diffractometer (Xpert PRO MPD) using $Cu_{K\alpha}$ radiation. The shape and size distribution of the nanoparticles were investigated using scanning electron microscope (SEM, KYKY-EM3900M). The magnetic properties of the samples were determined by vibrating sample magnetometer (VSM, model MDK, Iran).

4 Results and discussion

4.1 XRD patterns

One of the goals of this research is to understand the effect of substituting of different Ce concentrations on the structural properties of Mn ferrite nanoparticles.

Figure 1 shows the XRD patterns of $MnCe_xFe_{2-x}O_4$ ($x = 0.0$, 0.6, 1.4) nanoparticles annealed at 700 °C. The peaks at 18.31°, 30.19°, 35.50°, 43.09°, 57.02°, and 62.49° are consistent with card no. 0465-017-00. The intense peak at 35.50° is related to (311) plane. The figure confirms that the diffraction peaks were sharp because of the nanometer size of the crystallites. The single-phase cubic spinel structure of undoped $MnFe_2O_4$ is clearly observed in the XRD patterns which is consistent with the results of Muthuraman et al. [10] and Islam et al. [6].The patterns also show that all the samples had formed the cubic single spinel phase. The size of the crystallites was determined by measuring

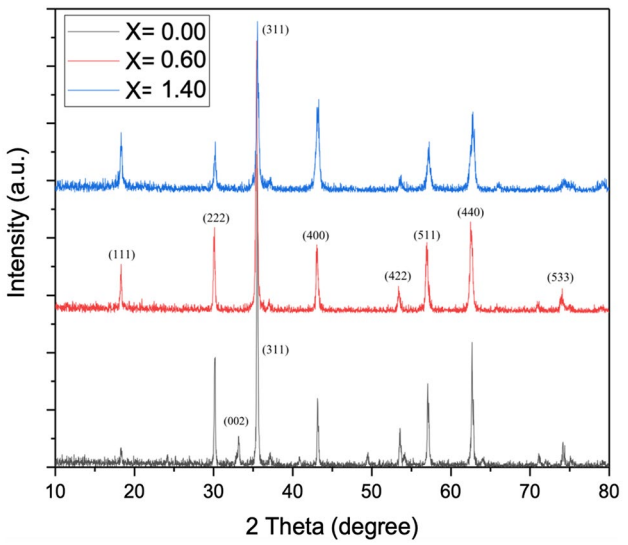

Fig. 1 XRD patterns of $MnCe_xFe_{2-x}O_4$ ($x=0.0$, 0.6, 1.4) nanoparticles annealed at 700 °C

Table 1 Variation of lattice constant and crystallite size with Ce concentration

Formula	Ce concentration	Lattice Constant (Å)	Mean crystallite size (nm)
$MnCe_xFe_{2-x}O_4$	$x=0.0$	8.37	60.44
	$x=0.6$	8.39	45.18
	$x=1.4$	8.37	26.90

FWHM of the most intense (311) diffraction peak using Debye Scherrer Eq. (1) [12].

$$D = \frac{0.9\lambda}{\beta \cos\theta} \tag{1}$$

where D is the size of the crystallite in nanometer, θ is the peak position (Bragg angle), λ is X-ray wavelength ($\lambda = 1.54056$ Å), and β is the full-width of the peak at half maximum (FWHM) in radian. The mean crystallite sizes of the samples are given in Table 1.The lattice parameter (a) (Å) was determined using Bragg's law (2) [10].

$$a = d_{hkl}\sqrt{h^2 + k^2 + l^2} \tag{2}$$

where d is the interplanar spacing, and h, k, *l* are the Miller indices of the mentioned planes. The lattice constants for all the prepared samples are also listed in Table 1. It can be seen that the lattice constants of individual phases did not change significantly by increasing the Ce concentration.

Further, the XRD patterns show the narrow reflections were exhibited due to the narrow size crystallites. The mean crystallite size of the samples lies in the range of 26.90 nm to 60.44 nm. The lattice parameter shows an increase for $x=0.6$ and then decreases for $x=1.4$. Since Ce ions have larger ionic radius (1.02 Å) than Fe^{+3} ions (0.64 Å), the lattice becomes more distorted by increasing the dopant concentration up to $x=0.6$, leading to higher lattice parameter. By further increasing the concentration beyond $x=0.6$, the lattice parameter decreases mainly due to the lower solubility of cerium ions compared to Fe^{+3} ions. This may also be due to the higher bonding energies of CeO_2 in the spinel structure compared to iron oxide. These results are in good agreement with Meena et al. [12] and Kamran et al. [13]. The impure peak observed at about 32° for x = 0.0 can be associated with α-Fe_2O_3 phase.

4.2 Morphological analysis

SEM was used to study the morphology of nanoparticles. Typical SEM micrographs of $MnCe_xFe_{2-x}O_4$ nanoparticles with $x=0.6$ and 1.4 prepared by sol–gel method after annealing at 700 °C are presented in Figs. 2a and b, respectively.

The annealing temperature of 700 °C was chosen as the optimum temperature, because the particles are almost spherical. The size of nanoparticles is less than 50 nm. The average size of nanoparticles in Fig. 2a is 40.61 nm. The nanoparticles in Fig. 2b are more uniform and distinguishable. The average size of these nanoparticles is 21.91 nm which is in good agreement with the crystallite size obtained from XRD patterns.

The surface morphology is clearly dependent on the cerium concentration. Figure 2a and b shows that by increasing the cerium concentration, the agglomeration and porosity of the particles vary without affecting the spherical morphology of the nanoparticles.

Field emission scanning electron microscopy (FESEM, MIRA, 3-TESCAN-XMU) images of $Ce_{1.4}MnFe_{0.6}O_4$ nanoparticles annealed at 700 °C were also obtained (at 15 kV and 150 KX), as shown in Fig. 2c and d. Size distribution histogram of the nanoparticles is shown in Fig. 3. The solid line corresponds to the best fit of the data. It can be seen that the mean particle size of the $MnCe_{1.4}Fe_{0.6}O_4$ nanoparticles is 30.53 nm. The results are almost equal to the crystallite sizes calculated according to Scherer equation.

4.3 Magnetic measurements

VSM was used to study the magnetic properties of $MnCe_xFe_{2-x}O_4$ ($x=0.0$, 0.6, 1.4) nanoparticles. The magnetic hysteresis loops were measured at room temperature (RT) with maximal applied magnetic field of 1 T. Figure 4 shows magnetic hysteresis loops of the nanoparticles after annealing at 700 °C. It is clear that the soft ferromagnetic properties of $MnCe_xFe_{2-x}O_4$ nanoparticles depend on the Ce concentration. At this step, the samples were labeled as

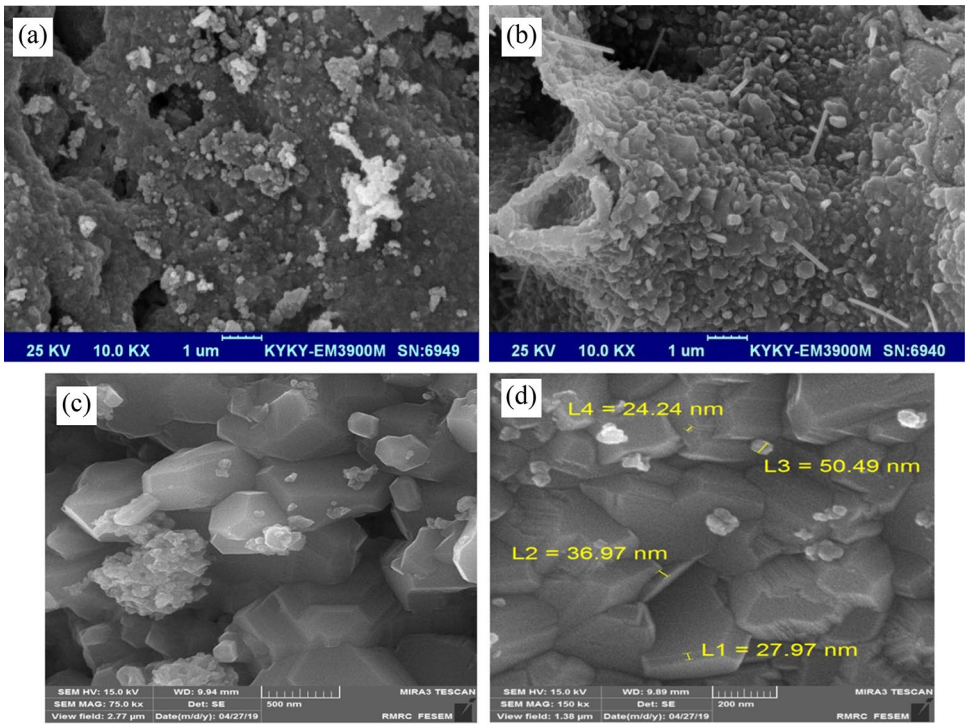

Fig. 2 SEM images of $MnCe_xFe_{2-x}O_4$ nanoparticles with **a** $x=0.6$, and **b** $x=1.4$ (25 kV, 10.0 KX). FESEM images of $Ce_{1.4}MnFe_{0.6}O_4$ nanoparticles: **c** 500 nm, and **d** 200 nm

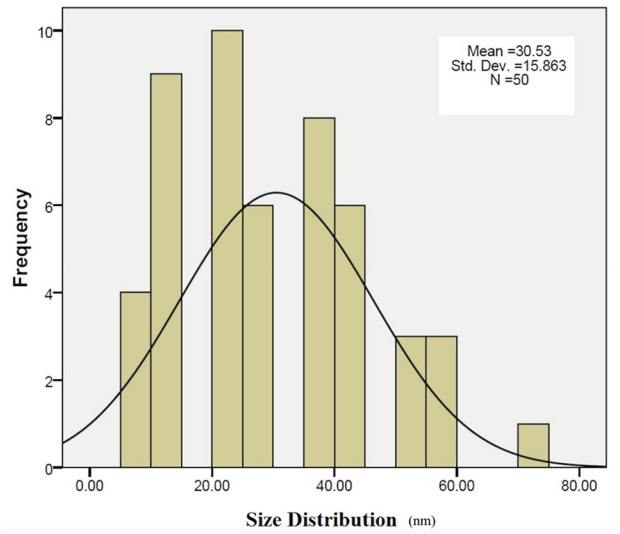

Fig. 3 Size distribution obtained from FESEM images of $Ce_{1.4}MnFe_{0.6}O_4$ nanoparticles

$MnFe_2O_4$ (S_4), $MnCe_{0.6}Fe_{1.4}O_4$ (S_5), and $MnCe_{1.4}Fe_{0.6}O_4$ (S_6).

Different magnetic properties such as coercivity (H_c), saturation magnetization (M_s), and remanent magnetization (M_r) were measured for $MnCe_xFe_{2-x}O_4$ ($x=0.0$, 0.6, and 1.4) nanoparticles based on the magnetization loops shown in Fig. 4. It can be seen from Table 2 that the saturation magnetization, remanent magnetization, and coercivity decrease with the addition of Ce. Elayakumar et al. [14] mentioned that the reduction in the saturation magnetization with increasing cerium content makes the Ce^{3+} substituted cobalt ferrites $CoCe_xFe_{2-x}O_4$ most suited for many technological potential such as the field of antenna construction and for reducing the size of the antenna.

M-H curve (Fig. 4a) for $MnCe_xFe_{2-x}O_4$ nanoparticles with $x=0.0$, i.e., $MnFe_2O_4$, indicates that its saturation magnetization is 60.69 emu/g for the particle size of 60.44 nm at RT with an applied magnetic field of 1 T. Saturation magnetization of bulk manganese ferrite is 80 emu/g [11, 15, 16]. The smaller M_s value of $MnFe_2O_4$ with respect to the bulk may be due to the higher percentages of atoms located on the surface of nanoparticles.

4.4 Energy dispersive X-ray (EDX)

Figures 5 and 6 show EDX spectra of $MnCe_xFe_{2-x}O_4$ with $x=0.0$ and $x=1.4$, respectively. The concentration (weight percent and atomic percent) of the main elements presented in these two samples is also listed in Tables 3 and 4, respectively.

EDX spectrum in Fig. 6 shows the presence of cerium in the sample, confirming that Ce-doped $MnFe_2O_4$ has been successfully synthesized via sol–gel method.

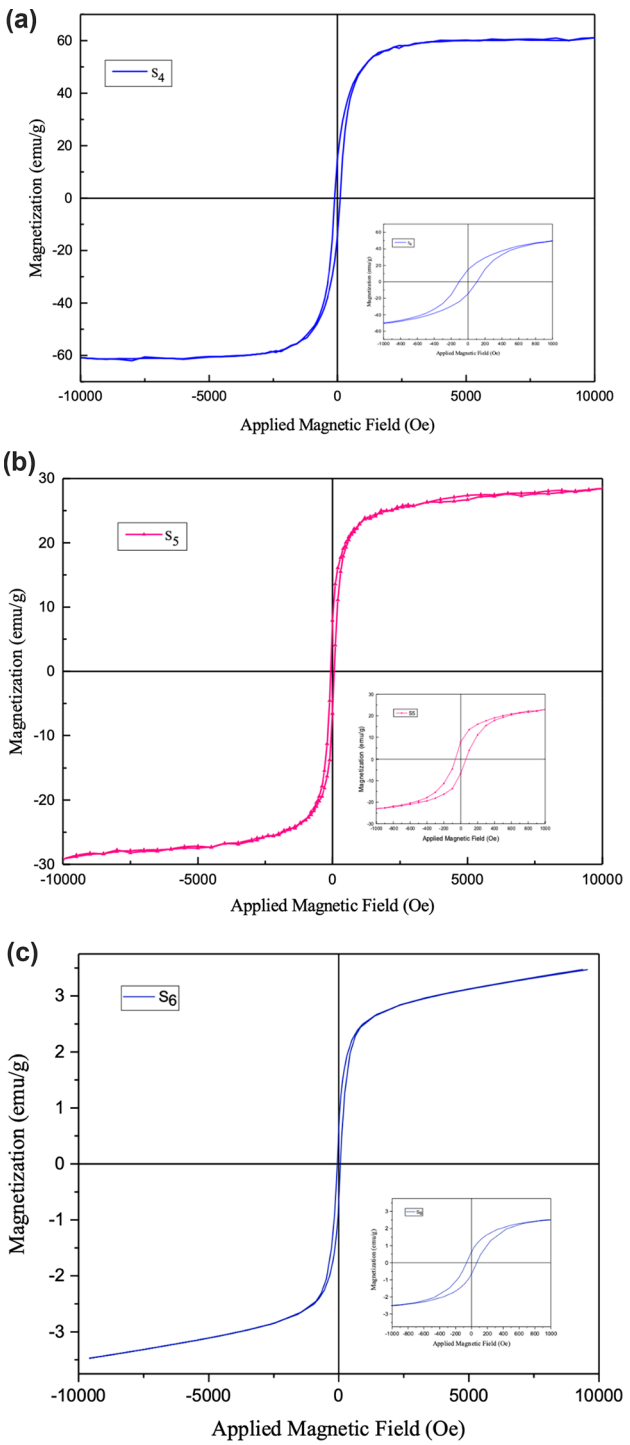

Fig. 4 a Magnetization loop of **a** $MnFe_2O_4$ (S_4), **b** $MnCe_{0.6}Fe_{1.4}O_4$ (S_5), and **c** $MnCe_{1.4}Fe_{0.6}O_4$ (S_6) samples

4.5 Evaluation of antifungal activities

The in vitro inhibitory potential of $MnFe_2O_4$ and $MnCe_{1.4}Fe_{0.6}O_4$ nanoparticles was studied against fungal pathogens (i.e., *Candida albicans*, *Aspergillus fumigates*, and *Fusariumoxysporum*), Gram-negative pathogenic bacteria (i.e., *Escherichia coli*, *Acinetobacterbaumannii*, and *Pseudomonas aeruginosa*), and Gram-positive pathogenic bacteria (i.e., *Bacillus cereus*, *Staphylococcus epidermidis*, and *Streptococcus pneumonia*). The results were reported as the minimum inhibitory concentration (MIC) and the minimum fungicidal concentration (MFC) values (Table 5). Antifungal drugs, i.e., terbinafine hydrochloride and fluconazole, were used as positive controls. Both $MnFe_2O_4$ and $MnCe_{1.4}Fe_{0.6}O_4$ NPs were not able to block the growth of the tested bacterial strains even at concentrations of 1024 µg mL^{-1}.

MIC and MFC values within the range of 256–512 µg mL^{-1} were recorded for $MnCe_{1.4}Fe_{0.6}O_4$ NPs against all the pathogens. Metal oxide NPs can inhibit the growth of microorganisms via outer membrane and cell wall destruction, generation of reactive oxygen species, metal-ion release, and particle internalization [17]. It is predicted that the presence of cerium ion in the structure of $MnCe_{1.4}Fe_{0.6}O_4$ nanoparticle is a major contributor to the antifungal activity. Cerium ions can cause oxidative stress of components of cell membrane of fungi, particularly *Candida albicans* [18]. The pH value on the cell membrane increases due to the reduction of Ce^{4+} to Ce^{3+}, resulting in higher vascular permeability.

As can be seen from Table 5, no inhibitory activity was observed for $MnFe_2O_4$ NPs. Antimicrobial effects of NPs can be varied according to the type of carrier and species diversity, size and morphology of particles, as well as the nature of growth media. Manganese ferrite nanoparticles synthesized by Lopez-Abarrategui et al. did not show antifungal activity against *Candida albicans* [19]. Antifungal effects were observed when they were conjugated with citric acid or 12 aa peptide. It is believed that undoped $MnFe_2O_4$ is unable to generate reactive oxygen species via oxidation of water molecules. Even though $MnFe_2O_4$ NPs prepared with average crystallite size of 16 and 23 nm could inhibit *Candida albicans* strains [20]. This is probably due to the differences in the morphology of particles.

Table 2 magnetic properties of $MnCe_xFe_{2-x}O_4$ samples with different Ce concentrations

Formula	Ce concentration	M_s (emu/g)	M_r (emu/g)	M_r/M_s	H_c (Oe)
$MnCe_xFe_{2-x}O_4$	$x=0.0$	60.69	14.77	0.24	109.61
	$x=0.6$	28.37	8.76	0.30	68.31
	$x=1.4$	3.47	0.53	0.15	63.38

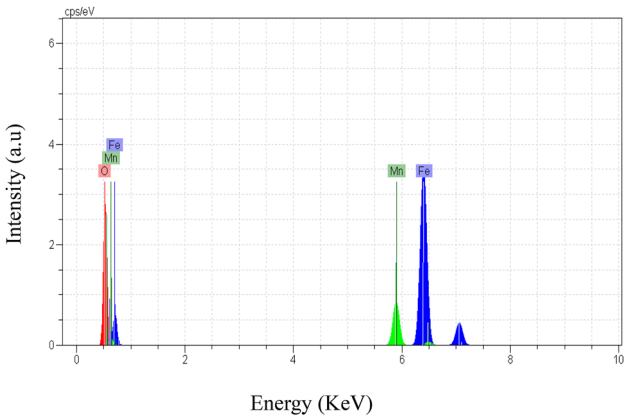

Fig. 5 EDX spectrum of $MnCe_xFe_{2-x}O_4$ with $x=0.0$

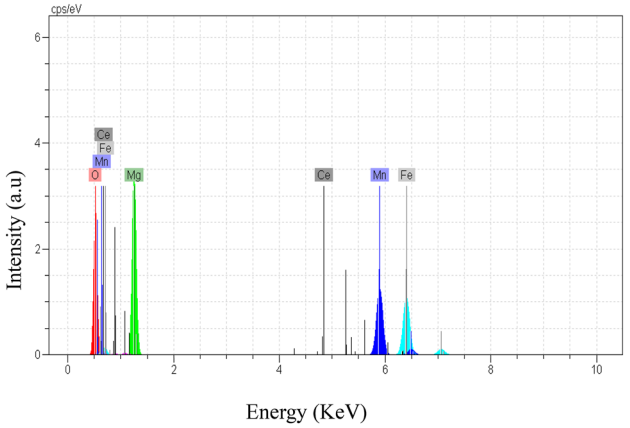

Fig. 6 EDX spectrum of $MnCe_xFe_{2-x}O_4$ with $x=1.4$

5 Conclusion

Manganese-cerium ferrite nanoparticles with different Ce concentrations were prepared by sol–gel method. The samples were analyzed using X-ray diffraction (XRD), scanning electron microscopy (SEM), field emission SEM (FESEM), and vibrating sample magnetometry (VSM) to obtain information on the sample phases, crystalline size, surface morphology, and magnetic properties of the samples. All the XRD peaks were indexed and the lattice constant (Å) was calculated for each Ce concentration. The crystallite size (nm) showed a decreasing trend with an increase in the Ce concentration. XRD patterns confirmed the presence of cubic α- Fe_2O_3 phase. Crystallite size of samples calculated using the Scherrer formula was in the range of 26.90 to 60.44 nm. SEM images showed that the particles are at the nanometer scale. EDX spectra revealed the presence of Ce in the composition, confirming the successful doping of Ce in the spinel structure. Magnetization curves revealed ferromagnetic behavior of $MnCe_xFe_{2-x}O_4$ ($x=0.0$, 0.6, 1.4) nanoparticles. Pathogenic fungi cause infectious diseases in human, animals and plants. The results showed that the synthesized $MnCeFe_2O_4$ nanoparticles can effectively block the growth of both pathogenic yeast and mold. According to their inhibitory effects against *Fusariumoxysporum*, they can be considered as suitable fungicidal candidates. In addition, they can be applied in water treatment due to their low solubility.

The results can be summarized as follows:

1) $MnCe_xFe_{2-x}O_4$ (x = 0.0, 0.6, 1.4) nanoparticles were synthesized via sol–gel method and their chemical, struc-

Table 3 Concentration of elements in $MnCe_xFe_{2-x}O_4$ sample with $x=0.0$

Elements	Weight percent	Atomic percent
Oxygen	24.35	53.25
Manganese	11.31	7.20
Iron	63.14	39.55

Table 4 Concentration of elements in $MnCe_xFe_{2-x}O_4$ sample with $x=1.4$

Elements	Weight percent	Atomic percent
Oxygen	26.09	49.38
Cerium	0.51	0.11
Manganese	25.13	13.54
Iron	30.65	16.25

Table 5 Antifungal activity of nanoparticles

Fungi	Inhibitory activity (μg mL^{-1})	NPs	Antifungal drugs		
	$MnFe_2O_4$	$MnCe_{1.4}Fe_{0.6}O_4$	Terbinafine		Fluconazole
Candida Albicans	MIC	–	512	32	256
	MFC	–	512	64	512
FusariumOxysporum	MIC	–	512	32	128
	MFC	–	512	64	256
Aspergillus Fumigatus	MIC	–	256	32	32
	MFC	–	256	32	64

tural, and magnetic properties were studied using XRD, SEM, FESEM, EDX and VSM.

2) The synthesized $MnCeFe_2O_4$ nanoparticles can effectively block the growth of both pathogenic yeast and molds. According to their inhibitory effects against *Fusariumoxysporum*, they can be considered as suitable fungicidal candidates.
3) In addition, they can be applied in water treatment due to their low solubility.

Acknowledgements The authors are thankful the referees for their suggestions to bring the first edition of the paper in the present form and they are highly thankful to the Sistan and Baluchestan University and Zabol University, Iran.

References

1. K.H.J. Buschow, *Magnetic Materials* (University of Amsterdam, The Netherlands, 2015)
2. A. Goldman, *Modern Ferrite Technology* (Van Nostrand Reinhold, New York, 1990)
3. R. Langer, New methods of drug delivery. Science **249**, 1527 (1990)
4. S. Rehman, M.A. Almessiere, N. Tashkandi, A. Baykal, Y. Slimani, R. Jermy, V. Ravinayagam, C. Yaman, Fabrication of spinel cobalt ferrite ($CoFe_2O_4$) nanoparticles with unique earth element cerium and neodymium for anticandidal activities. Chem. Sel. **4**(48), 14329–14334 (2019)
5. J. Judith Vajaya, G. Sekaran, M. Bououdina, Ceram. Int. (2015). https://doi.org/10.1016/j.ceramint.2013.10.145
6. K. Islam, M. Haque, A. Kumar, A. Hoq, F. Hyder, S. Manjura-Hoque, Nanomaterials (2020). https://doi.org/10.3390/nano10112297
7. I.T. Weber, A.P. Maciel, P.N. Lisboa-Filho, C.O. Paiva-Santos, W.H. Schreider, Y. Maniette, E.R. Leite, E. Longo, Nano Lett. **2**, 969 (2002)
8. E.R. Leite, A.P. Maciel, I.T. Weber, P.N. Lisboa-Filho, E. Longo, C.O. Paiva-Santos, W.H. Schreider, Y. Maniette, C.A. Pascocimas, A.V.C. Andrade, Adv. Mater. **14**(12), 905 (2002)
9. J.T. Dahle, Y. Arai, Int. J. Environ. Res. Public Health (2015). https://doi.org/10.3390/ijerph120201253
10. K. Muthuraman, V. Naidu, S.K. Ahamed, T. Vasudev, Int. J Comput. Appl. **65**, 23 (2013)
11. P. Mathura, A. Thakura, M. Singha, J. Magn. Magn. Mater. **320**, 1364–1369 (2008)
12. S. Meena, K.S. Anantharaju, Y.S. Vidya, L. Renuka, B. Uma, S.C. Sharma, B.S.S. Daruka Prasad et al., Ceram. Int. (2021). https://doi.org/10.1016/j.ceramint.2020.11.105
13. M. Kamran, M. Anis-ur-Rehman, J. Alloys Compd. **822**, 153583 (2020)
14. K. Elayakumar, A. Dinesh, A. Manikandan, M. Palanivelu, G. Kavitha, S. Prakash, R. Thilak Kumar, S.K. Jaganathan, A. Baykal, Structural, morphological, enhanced magnetic properties and antibacterial bio-medical activity of rare earth element (REE) Cerium (Ce^{3+}) doped $CoFe_2O_4$ nanoparticles. J. Magn. Magn. Mater. **476**, 157–165 (2019)
15. Q. Li, C.F. Conde, A. Conde, L.F. Kiss, Phys. Rev. B**72**(2005)
16. T. Suominen, J. Raittila, T. Salminen, K. Schlesier, J. Linden, P. Paturi, J. Magn. Magn. Mater. **309**, 278–284 (2007)
17. H. Beyzaei, M. KamaliDeljoo, R. Aryan, B. Ghasemi, M.M. Zahedi, M. Moghaddam-Manesh, Chem. Cent. J. **12**, 114 (2018)
18. S. Stankic, S. Suman, F. Haque, J. Vidic, J. Nanobiotechnol. **14**, 73 (2016)
19. I. Albuquerque, P. Farias, C. Christiano Lima dos Santos, F. Correia Sampaio, Bio Med. Res. Int. (2018). https://doi.org/10.1155/2018/1923606
20. A.M. Jacintha, V. Umapathy, P. Neeraja, S. RexJeyaRajkumar, J. Nanostruct. Chem. (2017). https://doi.org/10.1007/s40097-017-0248-z